Bond Characterization of Metal Squarate Complexes $[M^{II}(C_4O_4)(H_2O)_4$; M = Fe, Co, Ni, Zn]

Chi-Rung Lee,[†] Chih-Chieh Wang,[†] Ko-Chun Chen,[‡] Gene-Hsiang Lee,[‡] and Yu Wang*[,†,‡]

Department of Chemistry, National Taiwan University, Taipei, Taiwan, ROC, and Instrumentation Center, National Taiwan University, Taipei, Taiwan, ROC

Received: June 19, 1998; In Final Form: October 1, 1998

Tetraaqua metal squarate complexes, $M(C_4O_4)(H_2O)_4$, (M = Fe, Co, Ni, Zn), are known to have a polymeric chain structure with $C_4O_4^{2-}$ as a bridge (μ-2) ligand between two metal ions in the trans position. Each metal ion is bonded to two $C_4O_4^{2-}$ and four water molecules. They are all isostructural with space group *C*2/*c*. A complete Ewald sphere of data is measured at 120 K up to 2θ of 100−120° using Mo Kα radiation for each complex. Such carefully measured intensities are used to investigate the detailed electron density distribution in order to understand the chemical bonding and the d-orbital splitting of the metal ions subjected in such a ligand field. Results on the electron density distribution will be presented in the form of deformation density and of Laplacian maps. Deformation density will be presented in terms of experimental $\Delta\rho_{x-x}$, $\Delta\rho_{m-a}$ (multipole model), and of theoretical $\Delta\rho$ derived from the HF and DFT calculations. The interesting bent bond feature on the four-membered ring ligand $C_4O_4^{2-}$ is explicitly demonstrated by the deformation density distribution and the bond path of the cyclic carbon−carbon bond. The asphericity in electron density distribution around the metal ion is also clearly illustrated in these compounds both in the deformation density and in Laplacian of the density. The comparison on the series of 3d-transition metal complexes will be made not only by the deformation density distribution and by the Laplacian of the density but also by the d-orbital population and by the associated topological properties at the bond critical point. The total number of d-electrons from the experiments are 6.05, 6.88, 7.89, and 8.40, respectively, for Fe(II), Co(II), Ni(II), and Zn(II) ions in these compounds. A comparison between experiment and theory is made for the Ni complex.

Introduction

The electron density distribution of transition metal complexes has been investigated extensively using the single-crystal X-ray diffraction method during the last decade.[1−19] Systematic studies on the 3d-transition metal complexes are made for the purpose of understanding the trend of electronic structure around the metal ion. The electronic structures of hexaaquametal(II) ions[1−13] are of archetypal importance in understanding metal−ligand (oxygen) bonds. Ammonium metal Tutton salts, $(NH_4)_2[M^{II}(H_2O)_6](SO_4)_2$ (M^{II} = V,[15,20] Cr,[3] Mn,[14,21] Fe,[5,16,20] Co,[20] Ni,[1,22] Cu,[2,4,23,24] Zn[25]), have been studied by X-ray[1−6] and polarized neutron diffraction,[11−13] where detailed charge[1−6] and spin densities[11−13] are given. The extent of σ and π metal−water bonding, electron correlation effects, and spin−orbit coupling effects are also discussed.[1−6,11−13] The Jahn−Teller distortions are demonstrated in Cr(II)[3] and Cu(II)[2,4] complexes in comparison with the nondistorted Fe(II)[5] complex. These series of studies give a good example that by systematically varying the central 3d-transition metal in an isostructural environment, detailed information can be provided not only on the metal ligand bond but also on the crystal field effect exerted on the metal ions.

The squarate dianion, $C_4O_4^{2-}$, is a simple, interesting cyclic compound with aromaticity.[26−30] With four C−O partial double bonds, it is a potential bridging ligand with possible μ-2[26,27] to μ-4[28,30] bridging ligands between the metals. The intermolecular H-bond does play an important role in such complexes[26−32] as well as in the simple squaric acid.[33−39] There are symmetric and asymmetric H-bonds in the solid.[26−39] Detailed structural relationships for various metal squarate complexes are discussed in a recent report.[32] Three types of metal squarate complexes are known for the 3d-transition metals. They are $M(C_4O_4)(H_2O)_4$ (M = Mn, Fe, Co, Ni, Cu, Zn),[26,27] $M(HC_4O_4)_2(H_2O)_4$ (M = Mn, Fe),[31,32] and $M(C_4O_4)(H_2O)_2$ (M = Mn, Fe, Co, Ni, Cu, Zn).[28−30] Recently, additional types have been found in $Co_3(\mu_2\text{-}OH)_2(C_4O_4)_2(H_2O)_3$,[40] $[V(OH)(C_4O_4)(H_2O)]_2$,[41] and $[V(OH)(C_4O_4)]_2\cdot 4H_2O$.[41] For $M(C_4O_4)(H_2O)_4$ complexes, they are of the linear chain type, where each $C_4O_4^{2-}$ is coordinated with two metals in the trans position and each metal is again linked by two $C_4O_4^{2-}$. In the case of Mn, Fe, Co, Ni, and Zn,[26,27] they are isostructural. These complexes, in general, give good quality of diffraction data. Accurate charge density studies on a series of these transition metal complexes are undertaken in order to further our understanding on the metal−aqua and metal−squarate bonding as well as the crystal field effect on the d-orbital populations. It will provide a valuable comparison with those paralleling structures found in the metal Tutton salts[4−6] since both types of complexes have six M−O bonds at a roughly octahedral symmetry.

The bonding in the planar four-membered ring ligand with aromaticity is also an interesting feature to look into via the electron density distribution. Such a distribution will be compared with our recent work on a related ammonium salt $(Me_2NH_2)[H_3(C_4O_4)_2]$.[39]

* To whom all correspondence should be addressed.
[†] Department of Chemistry.
[‡] Instrumentation Center.

10.1021/jp982696c CCC: $18.00 © 1999 American Chemical Society
Published on Web 12/17/1998

TABLE 1: Crystal Data of $[M(C_4O_4)(H_2O)_4]$ (M = Fe, Co, Ni, Zn)

		Crystal Data		
chemical formula	$Fe(C_4O_4)(H_2O)_4$	$Co(C_4O_4)(H_2O)_4$	$Ni(C_4O_4)(H_2O)_4$	$Zn(C_4O_4)(H_2O)_4$
chemical formula weight	239.95	243.03	242.81	249.48
cell setting	monoclinic	monoclinic	monoclinic	monoclinic
space group	*C*2/*c*	*C*2/*c*	*C*2/*c*	*C*2/*c*
a, Å	9.032(1)	8.965(1)	8.913(3)	8.986(2)
b, Å	13.381(1)	13. 376(3)	13.232 (4)	13.333(2)
c, Å	6.734(2)	6.680(1)	6.654 (3)	6.694(3)
β, deg	99.19(2)	99.67 (1)	99.71 (3)	99.67(2)
V, Å^{-3}	803.0(3)	789.7(3)	773.4 (5)	790.6(3)
Z	4	4	4	4
D_x, Mg m^{-3}	1.984	2.044	2.085	2.096
radiation type	Mo Kα	Mo Kα	Mo Kα	Mo Kα
wavelength, Å	0.7107	0.7107	0.7107	0.7107
no. of reflns for cell parameters	25	25	25	25
2θ range for unit cell detn, deg	89−108	75−98	71−96	40−90
μ, cm^{-1}	18.9	21.8	25.3	31.9
temperature, K	120	120	120	120
crystal size, mm	0.15 × 0.15 × 0.3	0.36 × 0.20 × 0.20	0.25 × 0.15 × 0.15	0.33 × 0.2 × 0.25
		Data Collection and Reduction		
diffractometer	Nonius CAD4	Nonius CAD4	Nonius CAD4	Nonius CAD4
data collection control	$\theta/2\theta$ scan mode	$\theta/2\theta$ scan mode	$\theta/2\theta$ scan mode	$\theta/2\theta$ scan mode
2θ scan width, deg	$2(0.65 + 0.35 \tan \theta)$	$2(0.70 + 0.35 \tan \theta)$	$2(0.70 + 0.35 \tan \theta)$	$2(0.70 + 0.35 \tan \theta$
speed, deg min^{-1}	2.06, 8.14	2.06, 8.14	2.06, 8.14	2.06, 8.14
absorption correction	Gaussian integration	Gaussian integration	Gaussian integration	Gaussian integration
T_{min}	0.660	0.550	0.564	0.434
T_{max}	0.807	0.693	0.716	0.584
no. of measured reflns	22539	17952	19497	19653
no. of unique reflns	6082	5633	4054	4140
no. of observed reflns	4642	4071	3186	3237
criterion for observed reflns	$I > 2\sigma(I)$	$I > 2\sigma(I)$	$I > 2\sigma(I)$	$I > 2\sigma(I)$
R_{int}[a]	0.023	0.021	0.027	0.023
$2\theta_{max}$, deg	120	110	100	100
range of *h*, *k*, *l*	$-21 \rightarrow h \rightarrow 21$ $0 \rightarrow k \rightarrow 32$ $0 \rightarrow l \rightarrow 16$	$-20 \rightarrow h \rightarrow 20$ $0 \rightarrow k \rightarrow 30$ $0 \rightarrow l \rightarrow 15$	$-19 \rightarrow h \rightarrow 18$ $0 \rightarrow k \rightarrow 28$ $0 \rightarrow l \rightarrow 14$	$-19 \rightarrow h \rightarrow 19$ $0 \rightarrow k \rightarrow 28$ $0 \rightarrow l \rightarrow 14$
no. of standard reflns	3	3	3	3
frequency of standard reflns	once per hour	once per hour	once per hour	once per hour
		Refinement		
refinement on	*F*	*F*	*F*	*F*
R[a]	0.024	0.023	0.025	0.024
R_w[a]	0.024	0.026	0.025	0.024
S[a]	2.91	2.84	2.54	2.47
no. of reflns used in refinement	4642	4071	3186	4140
no. of parameters used	78	78	78	78
H-atom treatment	difference Fourier	difference Fourier	difference Fourier	difference Fourier
weighting scheme	$1/[\sigma^2(F_o) + 10^{-5}(F_o^2)]$	$1/[\sigma^2(F_o) + 10^{-5}(F_o^2)]$	$1/[\sigma^2(F_o) + 10^{-5}(F_o^2)]$	$1/[\sigma^2(F_o) + 10^{-5}(F_o^2)]$
$(\Delta/\sigma)_{max}$	0.0006	0.064	0.002	0.001
$\Delta\rho$ max, e Å^{-3}	0.92	0.95	1.29	0.79
$\Delta\rho$ min, e Å^{-3}	−1.03	−1.04	−0.98	−1.13
extinction method	secondary (Larson, 1970)[68]	secondary (Larson, 1970)[68]	secondary (Larson, 1970)[68]	secondary (Larson, 1970)[68]
extinction coefficient × 10^4	0.29(1)	0.125(9)	0.086(2)	0.202(9)
source of atomic scattering factors	*International Tables for X-ray Crystallography* (1974, Vol. IV)	*International Tables for X-ray Crystallography* (1974, Vol. IV)	*International Tables for X-ray Crystallography* (1974, Vol. IV)	*International Tables for X-ray Crystallography* (1974, Vol. IV)
computer program used	NRCVAX[40]	NRCVAX[40]	NRCVAX[40]	NRCVAX[40]

[a] $R = \sum|F_o - F_c|/\sum F_o$. $R_w = [\sum w|F_o - F_c|^2/\sum wF_o^2]^{1/2}$. $R_{int} = \sum|I_i - \langle I\rangle|/\sum I_i$. $S = [\sum w|F_o - F_c|^2/(NR - NV)]^{1/2}$; NR = no. of reflns, NV = no. of variables.

Experimental Section

Data Collection. Title compounds were synthesized according to the literature.[26,27] Suitable single crystals were obtained by direct crystallization out of aqueous solution. Each crystal was sealed in a glass capillary tube for data measurement. Intensity data were collected using Mo Kα radiation at 120 K with a liquid nitrogen device. A full sphere of reflections (four equivalent sets) was collected, and an absorption correction was applied before the averaging of equivalents based on the face measurements. The correctness of the absorption correction was checked against the experimental ψ curves for a few adequate reflections. The interset agreement was reasonable for all four complexes. Each reflection was then corrected for Lorentz and polarization effects. Three standard reflections were monitored every hour throughout the data measurement; the variation in intensity was all within ±5%. Other details are listed in Table 1.

Refinement. Conventional refinements are performed[42] with the full-matrix least-squares process both on full data and on high-order data ($\sin\theta/\lambda \geq 0.6$). The standard deviation of the average intensity is taken from the geometric mean of the equivalents. Results of the refinements are also given in Table 1.

Additional multipole refinements are performed with the MOLLY program,[43] where all the multipolar terms are expressed as a series expansion of the spherical harmonic functions. A multipole model is such that the atomic density is expressed as the sum of a core density, a spherical valence density, and a series of spherical harmonic terms with variable population, P_{lmp}, to describe the nonspherical feature of atomic electron density. The exact expression[43] is

$$\rho(\mathbf{r}) = \rho_{\text{core}} + \kappa^3 P_{\text{valence}}\rho_{\text{valence}}(\kappa r) + \sum_{n=0}^{l} R_{n,l}(r) \sum_{m=0,p=\pm}^{+l} P_{lmp} y_{lmp}(\mathbf{r}/r)$$

$$R_{n,l}(r) = N r^{n_l} \exp(-\zeta_l r)$$

where ρ_{core} and ρ_{valence} are spherical core and valence densities, respectively, κ is a radial contraction−expansion parameter, y_{lmp} is the spherical harmonic angular function in real form, $R_{n,l}$ is the radial part of the function where N is a normalization factor, and n_l and ζ_l are chosen for each l value.[43] P_{valence}, P_{lmp}, and κ are refinable parameters in addition to the atomic positional and vibrational parameters. Multipole terms up to hexadecapoles are included for metal ions; up to octapole are included for carbon and oxygen atoms, and up to dipole is for the hydrogen atom. The core and valence scattering factors for each atom are taken from *International Tables for X-ray Crystallography* (1974, Vol. IV). The core electron configurations are assumed to be He core for O and C; Ca core for all metal atoms.

Deformation Density Maps. Three types of experimental deformation density maps are presented in this work. The first one is the experimental $\Delta\rho_{\text{x-x}}$, where Fourier coefficients are obtained from the difference between F_o and F_c. F_c is calculated based on the parameters obtained from the high-order ($\sin\theta/\lambda \geq 0.6$) refinements. H atoms are moved along O−H vectors to make an O−H distance of 0.957 Å.[44] The second one is a model deformation density map $\Delta\rho_{\text{m-a,dynamic}}$, which is derived from a multipole model where Fourier coefficients are differences between two F_c values—one derived from a multipole model shown above, the other being the first two terms of the equation (spherical part) but with P_{valence} set to be neutral atom and κ reset to 1. The third one is a static model ($\Delta\rho_{\text{m-a,static}}$), which is obtained by plotting the density of each atom in direct space according to the equation given above, where no nuclear vibrations are taken into account. To check the correctness of the model deformation density, a residual density map $\Delta\rho_{\text{res}}$ is normally generated after the multipole refinement. This map is the difference density between the observed and the multipole model density. Deformation density distribution of [Ni(C_4O_4)(H_2O)$_4$] is also investigated with theoretical calculations based on the ab initio method at the HF level and on the density functional (DFT) method, where the sum of atomic densities is subtracted from the molecular densities.

A critical point (CP), r_c, is a point in space that satisfies the condition of $\nabla\rho(r_c) = 0$. The Laplacian of the density can be obtained from the second derivative of the total electron density, $\nabla^2\rho$. When $\nabla^2\rho(r) < 0$, the electron density is locally concentrated at r; when $\nabla^2\rho(r) > 0$, the electron density is locally depleted at r. In addition, the Laplacian value and the eigenvalues of the Hessian matrix (λ_1, λ_2, λ_3) at the bond critical point (BCP) (3, −1) provide a description of the interaction between the bonded atoms as being either closed shell (ionic) or shared (covalent) interaction. The electron density at BCP, $\rho(r_c)$, is a direct indicator of the bond order. The Fermi hole function is an effective tool for recognizing the electron delocalization. Detailed definitions of all these topological properties are given elsewhere.[45,46]

TABLE 2: Non-Hydrogen Atomic Parameters and Equivalent Isotropic Thermal Parameters (Å^2) with Esd's in Parentheses for the Structures of M(C_4O_4)(H_2O)$_4$ (M = Fe, Co, Ni, and Zn) at 120 K

		Fe	Co	Ni	Zn
M	*x*	0.75	0.75	0.75	0.75
	y	0.25	0.25	0.25	0.25
	z	0.0	0.0	0.0	0.0
	B_{iso}	0.529(2)	0.547(2)	0.499(3)	0.544(3)
O1	*x*	0.94979(4)	0.94684(4)	0.94523(5)	0.94649(6)
	y	0.16732(3)	0.16711(3)	0.16855(4)	0.16751(4)
	z	0.01120(7)	0.00858(7)	0.01018(9)	0.01044(9)
	B_{iso}	0.74(1)	0.77(1)	0.71(1)	0.73(1)
O2	*x*	0.25180(5)	0.24897(4)	0.25034(6)	0.24862(6)
	y	0.04002(3)	0.04179(3)	0.04283(4)	0.04224(4)
	z	0.00868(7)	0.00549(7)	0.00915(9)	0.00876(9)
	B_{iso}	0.80(1)	0.86(1)	0.80(1)	0.80(1)
O3	*x*	0.62708(5)	0.62555(5)	0.62480(6)	0.62414(6)
	y	0.12399(3)	0.13005(3)	0.13198(4)	0.12993(4)
	z	0.10222(7)	0.09708(8)	0.09314(9)	0.09568(9)
	B_{iso}	0.89(1)	0.93(1)	0.85(2)	0.87(2)
O4	*x*	0.81971(5)	0.81848(5)	0.81642(7)	0.81800(7)
	y	0.28939(4)	0.28743(4)	0.28608(5)	0.28735(5)
	z	0.30268(7)	0.30083(7)	0.29854(9)	0.30149(9)
	B_{iso}	1.04(1)	1.09(1)	1.04(2)	1.05(2)
C1	*x*	0.97512(5)	0.97360(5)	0.97274(7)	0.97350(7)
	y	0.07529(3)	0.07522(3)	0.07581(4)	0.07533(5)
	z	0.00463(8)	0.00381(8)	0.0043(1)	0.0045(1)
	B_{iso}	0.55(1)	0.58(1)	0.55(2)	0.55(2)
C2	*x*	0.11260(5)	0.11308(5)	0.11361(7)	0.11282(7)
	y	0.01755(3)	0.01834(3)	0.01890(5)	0.01859(5)
	z	0.00431(8)	0.00309(8)	0.0048(1)	0.0045(1)
	B_{iso}	0.56(1)	0.60(1)	0.57(2)	0.56(2)

TABLE 3: Selected Bond Distances (Å) and Angles (deg) of M(C_4O_4)(H_2O)$_4$ (M = Fe, Co, Ni, and Zn)

	Fe	Co	Ni	Zn
Bond Distance (Å)				
M−O1(sq[a])	2.1076(4)	2.0767(4)	2.0381(7)	2.0714(6)
M−O3(wi[a])	2.1394(5)	2.1173(5)	2.0739(7)	2.1202(6)
M−O4(wo[a])	2.1021(7)	2.0619(6)	2.032(2)	2.069(1)
O1−C1	1.2546(6)	1.2538(6)	1.2532(8)	1.2546(8)
O2−C2	1.2569(7)	1.2555(6)	1.2547(9)	1.2561(8)
C1−C2	1.4627(7)	1.4645(6)	1.4636(9)	1.4628(9)
Bond Angle (deg)				
O1−M−O3	85.329(2)	85.64(2)	84.76(3)	85.19(2)
O1−M−O4	91.448(2)	90.56(2)	90.83(3)	90.88(3)
O3−M−O4	91.817(2)	91.64(2)	91.86(3)	91.60(3)
M−O1−C1	132.37(3)	133.48(3)	133.40(4)	133.43(5)
O1−C1−C2	132.70(5)	132.57(4)	132.53(6)	132.60(6)
O2−C2−C1	136.06(4)	136.05(5)	135.85(6)	135.99(6)
C1−C2−C1	89.68(4)	89.73(4)	89.75(5)	89.71(5)
C2−C1−C2	90.32(4)	90.27(4)	90.25(5)	90.29(5)

[a] wi: in-plane M−O_w. wo: out of plane M−O_w. sq: squarate.

Computational Detail. The model compound chosen for the calculation in the theoretical comparison is [Ni(HC_4O_4)$_2$(H_2O)$_4$]. The geometry is taken from the diffraction data. To simplify the computation, the polymeric geometry is broken into a monomer by replacing two μ-C_4O_4 ligands with the HC_4O_4 moiety. The molecular symmetry is C_i with the center of inversion at the metal ion. For both HF and DFT calculations, the functions used for the Ni atom are (14, 9, 6)/[8, 4, 3] contractions: (626*1/5112/411),[47,48] where the (14s, 9p) primitive Gaussian functions are taken from Wachters[48] and the (6d) basis set is from Goddard.[47] The basis sets used for the O, C, and H atom are 6-31G**. The nonlocal correction applied in DFT is B3PW91.[49−52] All these calculations are made using the Gaussian94 program.[53] Total electron density from the

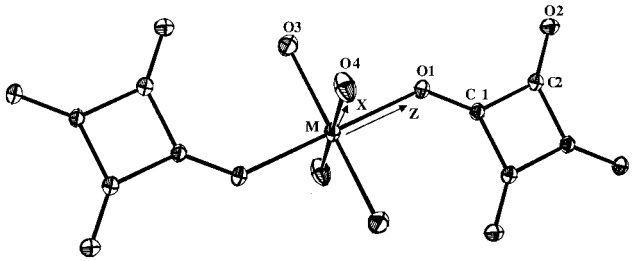

Figure 1. Molecular drawing with 50% probability in thermal ellipsoids at 120 K and choice of local Cartesian axis of metal centers.

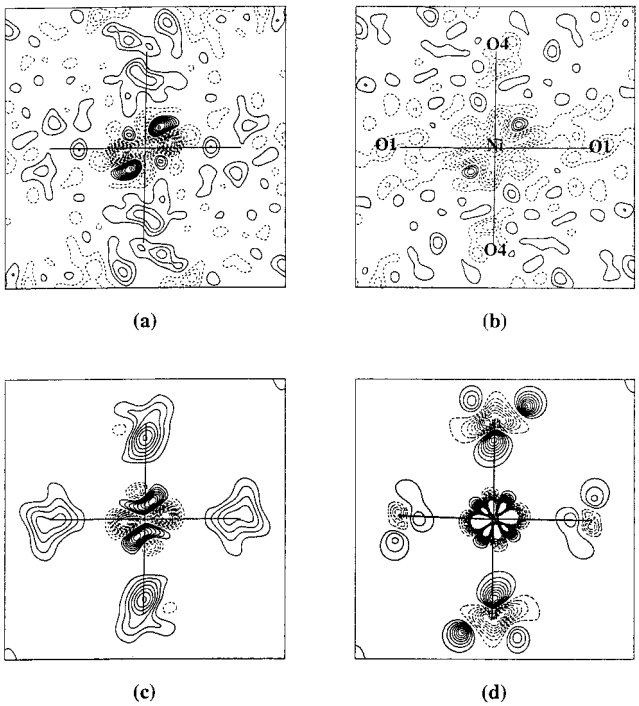

Figure 2. Deformation density maps of the O1−Ni−O4 plane, contours interval 0.1 e Å^{-3} within ±1.8 e Å^{-3}: (solid line) positive; (dashed line) negative; (a) $\Delta\rho_{x-x}$; (b) $\Delta\rho_{res}$; (c) $\Delta\rho_{m-a,dynamic}$; (d) $\Delta\rho_{m-a,static}$.

experiment is calculated on the basis of the multipole parameters.[43] Maps of Laplacian and the other topological properties are obtained using PROP[54] and AIMPAC[55] programs, respectively, for experiment and MO calculation.

Result and Discussion

Structure. The crystal structures at 120 K are the same as those at room temperature for all four complexes. They are isostructural in space group *C*2/*c*, and the metal is at the $\bar{1}$ site. The molecular structure and atomic coordinates obtained from full-matrix least-squares refinements are listed in Table 2. The metal ions are six-coordinated, with four aqueous (O_w) and two squarate (O_{sq}) oxygen atoms. Selected bond distances and bond angles are given in Table 3. The molecular structure, atomic labeling, and internal coordinates of the metal ion are shown in Figure 1. There are two M−O_w bonds, one (M−O3) is parallel to the C_4O_4 plane (in-plane), and the other (M−O4) is perpendicular to the C_4O_4 plane (out-of-plane). One finds that the in-plane M−O3 bond is much longer than the out-of-plane M−O4 bond and the M−O_{sq} bond. Therefore, the coordination of the metal ion in these complexes can be considered as a tetragonally distorted octahedron. However, the distortion is along one of the M−O_w (in-plane) directions. According to the literature,[27] this type of complex is more stable than the type

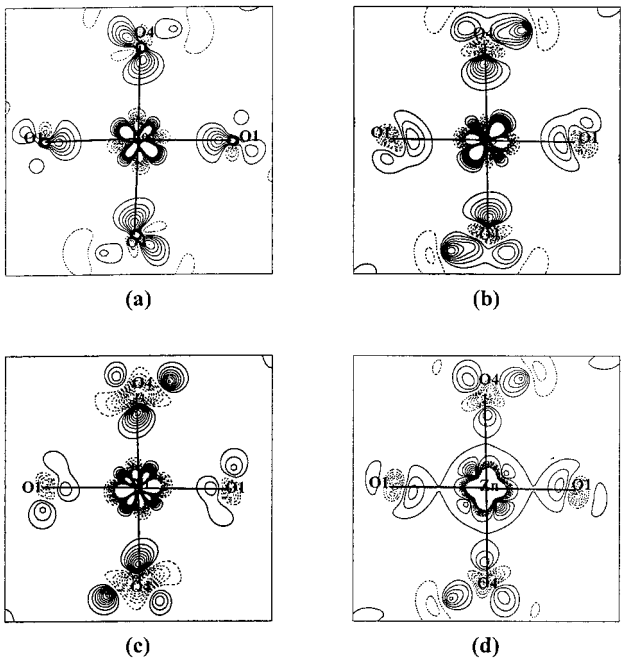

Figure 3. Deformation density maps of the O1−M−O4 and C_4O_4 ring plane: (a) Fe; (b) Co; (c) Ni; (d) Zn (in charge model). Contours are as in Figure 2.

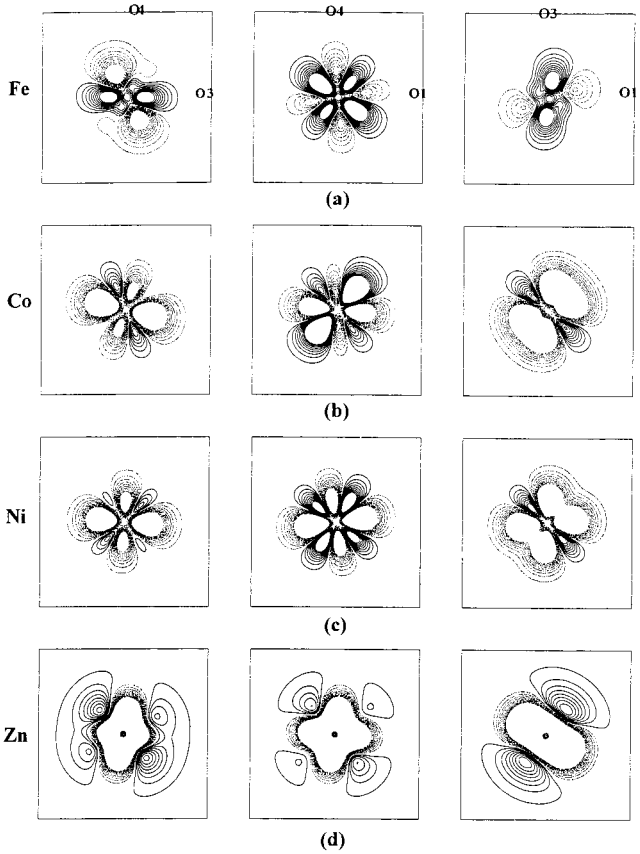

Figure 4. Deformation density maps of three unique planes (O3−M−O4, O1−M−O4, O1−M−O3) around the metal ion, contour interval 0.2 e Å^{-3} within ±1.8 e Å^{-3}: (a) Fe; (b) Co; (c) Ni; (d) Zn (in charge model), plot size 2 × 2 Å. The directions of O1, O3 and O4 are labeled in (a).

of $M(C_4O_4)(H_2O)_2$ at low temperature; presumably, the weaker in-plane M−O3 bond in the $M(C_4O_4)(H_2O)_4$ compounds is replaced by another M−O_{sq} bond and becomes $M(C_4O_4)(H_2O)_2$. According to bond distances of the M−O given in Table 3, the

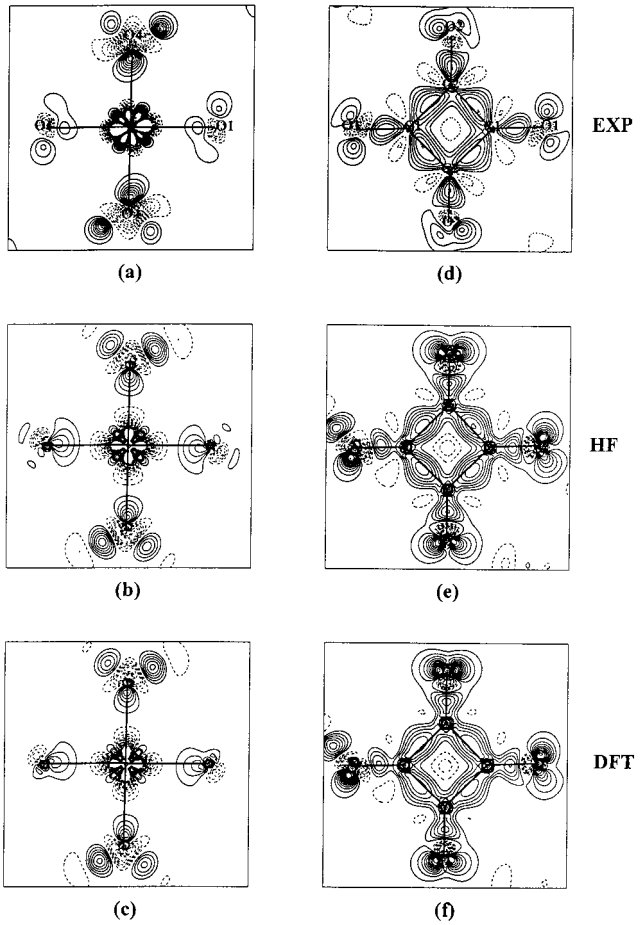

Figure 5. Deformation density maps of the O1−Ni−O4 plane (a−c) and C_4O_4 ring plane (d−f): (a) and (d) experiment; (b) and (e) HF; (c) and (f) DFT. Contours are as in Figure 2.

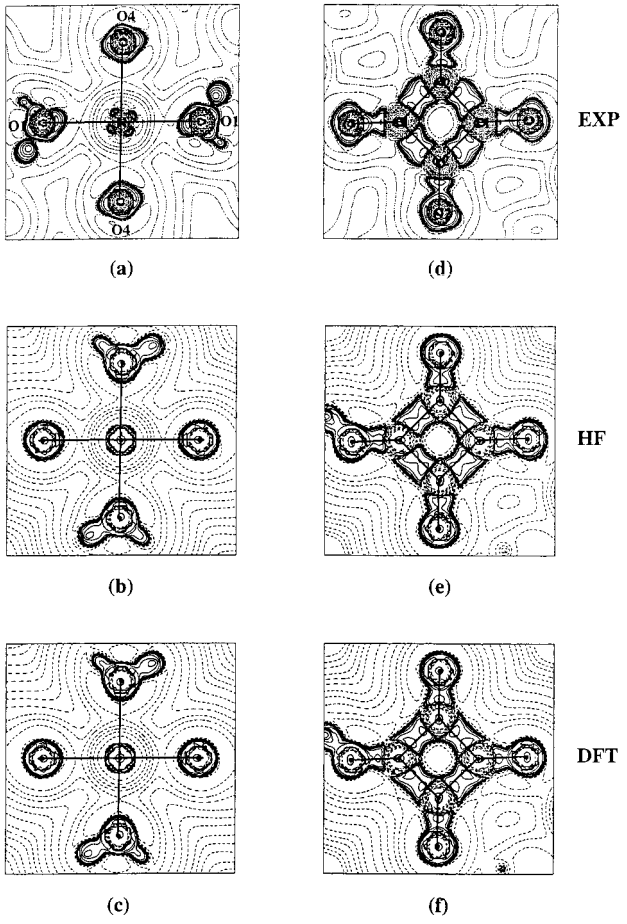

Figure 6. Negative Laplacian maps of the Ni complex: (solid line) positive; (dotted line) negative. The contour changes in steps of $(-1)^l 2^m 10^n$ ($l = 1, 0$; $m = 1-3$; $n = -3$ to $+3$). (a)−(d) are defined as in Figure 5.

TABLE 4: Agreement Indices of Various Refinements

	Fe	Co	Ni	Zn
NR[a]	4642	4071	3186	3237
		Conventional		
NV[b]	62	62	62	62
R	0.0262	0.0242	0.0260	0.0305
R_w	0.0316	0.0306	0.0294	0.0404
R_2[c]	0.0378	0.0385	0.0369	0.0440
R_{2w}[d]	0.0510	0.0482	0.0441	0.0601
S	3.858	3.355	2.921	4.209
		Monopole		
NV	76	76	76	76
R	0.0237	0.0226	0.0246	0.0235
R_w	0.0220	0.0246	0.0243	0.0221
R_2	0.0325	0.0344	0.0336	0.0352
R_{2w}	0.0347	0.0405	0.0365	0.0429
S	2.691	2.697	2.418	2.306
		Hexadecapole		
NV	192	192	192	192
R	0.0183	0.0170	0.0197	0.0189
R_w	0.0133	0.0165	0.0175	0.0156
R_2	0.0226	0.0231	0.0254	0.0267
R_{2w}	0.0194	0.0270	0.0270	0.0353
S	1.664	1.835	1.774	1.668

[a] NR: number of reflections. [b] NV: number of variables. [c] $R_2 = \sum|F_o^2 - F_c^2|/\sum F_o^2$. [d] $R_{2w} = (\sum w|F_o^2 - F_c^2|^2/\sum w|F_o|^4)^{1/2}$.

Fe−O bond length is the longest and the Ni−O is the shortest among the four complexes. This trend is exactly the same as those in Tutton salts[56] and other hexaaquametal ions.[6−8] The expected trend, predicted by ligand field theory (LFT) for these octahedral high-spin species, is such that the longest M−O distance should be found in manganese (d^5) and zinc (d^{10}) complexes and the shortest in vanadium (d^3) and nickel (d^8) complexes.[56] For the ligand part, the squarate dianion, $C_4O_4^{2-}$, is in a perfect D_{4h} symmetry with a C−O distance of 1.255 Å and a C−C distance of 1.463 Å. Weak H-bonds are found between water molecules and squarates of the neighboring chain.[32]

Deformation Density. Significant improvements on the agreement indices over the additional multipole terms are apparent in Table 4. This indicates that the multipole model does give a better representation of the electron density distribution than the spherical model does. For each complex, the deformation density distribution is calculated using $\Delta\rho_{x-x}$, $\Delta\rho_{m-a,dynamic}$, and $\Delta\rho_{m-a,static}$. The main features are quite similar between all these maps and the residual map $\Delta\rho_{res}$ is quite reasonable. One example for the Ni complex is displayed in Figure 2. For clarity, only the static maps are given for the other complexes. Static deformation density maps of a specific molecular plane, namely the plane passing through O1−M−O4, are depicted in Figure 3 for all the complexes. Four plots including three unique planes (O3−M−O4; O1−M−O4; O1−M−O3) around each metal ion are compared in Figure 4. The comparison of $\Delta\rho$ in the Ni complex between experiment and theory is shown in Figure 5, where one molecular plane (O1−M−O4) of the Ni complex and the plane of the squarate ligand are given. The maps of the ligand plane for all four complexes are nearly identical with the electron density accumulated at the bonding region of the C−O and C−C bonds and the lone

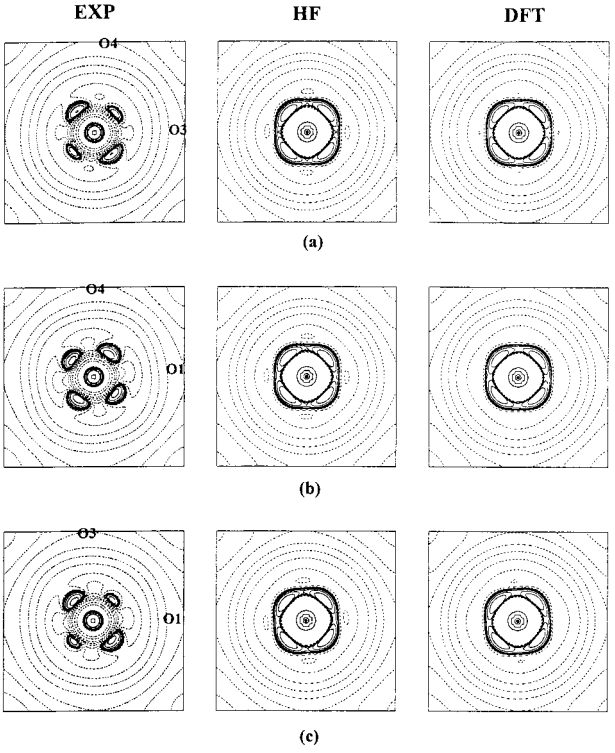

Figure 7. Negative Laplacian maps of the Ni complex obtained from experimental and theoretical results: (a) O3−M−O4; (b) O1−M−O4; (c) O1−M−O3 plane. Contours and plot size are as in Figure 6.

pair of the oxygen; one example is given in Figure 5d. It is also in good agreement with the corresponding map in $[H(HC_4O_4)_2^-]$,[39] although such an anion is actually in a dimeric form connected by a symmetric H-bond.[39] It is interesting to notice that the electron density distribution on the squarate plane clearly shows the ring strain of a four-membered ring. The analysis of $\Delta\rho$ (Figure 5d) provides a basis for a quantitative description of a "convex" bent bond expected for such a small ring compound.[39,57] The bonding electron density maximum is outward from the C−C interatomic axis (exocyclic) in the deformation density maps. It gives an angle of 110° between two bonding maxima at the carbon atom (C2) when the corresponding bond angle ∠C1−C2−C1′ is only ∼90°. This is consistent with the four-centered σ bond being composed of four tangentially oriented (t-set) p-orbitals.[39,57] However, the bent bond feature is not so pronounced in the theoretically calculated ones shown in Figure 5e,f. Similar observation is found in $[H_3(C_4O_4)_2^-]$.[39] The lone pair electrons of oxygen atoms are quite observable in the O1−M−O4 planes (Figure 3). The σ donor character of the lone pair electrons at oxygen toward the metal ion is obvious. Actually, all three O−M−O planes give the same feature in deformation density maps. The asphericity in density around the metal ion is apparent (Figure 4) with electron depletion along d_σ and electron accumulation along the d_π direction, which is expected in terms of simple crystal field theory; the only exception is found along the Fe−O3 bond, which happens to be the longest M−O bond in all these compounds. The same feature is also noticed in (ND_4)-$[M(D_2O)_6](SO_4)_2$ along the Fe−O[5] and Cu−O bond.[4] However, such asymmetric density distribution is usually not found in the theoretically calculated maps. The asymmetric distribution near the metal center is nevertheless found quite often in other experimental maps,[1−6,18] specially where the concerning bond angles differed substantially, in this case 85° vs 91°. The discrepancies may due to the effect of the thermal parameters

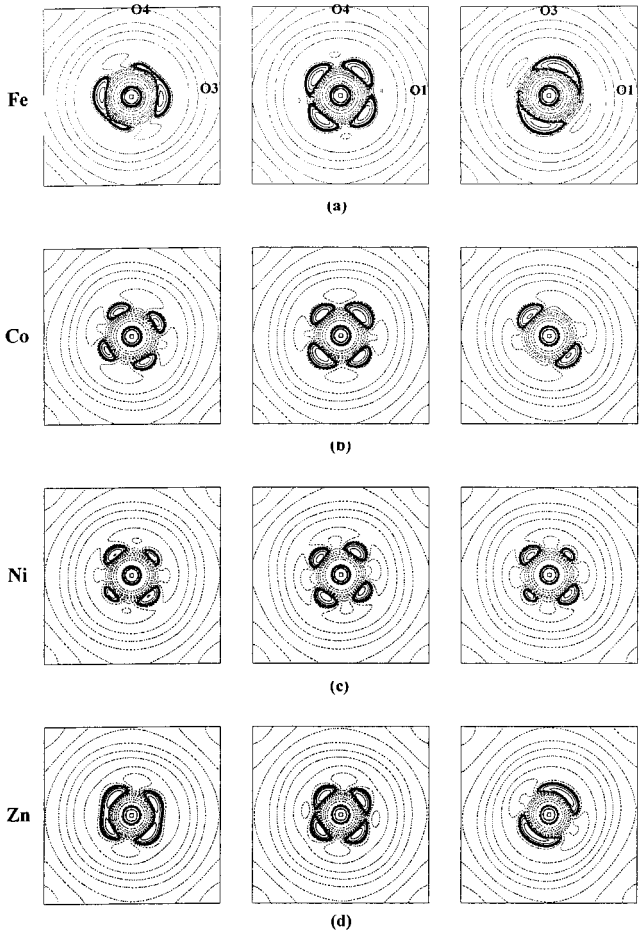

Figure 8. Negative Laplacian maps of the metal center from experimental results: (a) Fe; (b) Co; (c) Ni; (d) Zn. The directions of O1, O3, O4 are labeled in (a). Contours are defined as in Figure 6.

being not completely unbiased from the multipole coefficients even at 100 K.[58] The density distributions around the metal ions are very similar in shape; they correspond to high-spin configurations with t_{2g}-orbitals more populated than e_g-orbitals. Because of the high positive charge of the Zn atom (+1.97), the deformation density (Figure 4d) is derived by the subtraction of the charged atom instead of the neutral atom. The agreement between the experiment and theory on the Ni complex (Figure 5a−c) is reasonable. The agreement in the ligand part (Figure 5d−f) is very good.

Laplacian and Bond Critical Points. The local density accumulation and depletion, or the valence shell charge concentration (VSCC), can also be realized via a Laplacian of the density, $\nabla^2\rho$. The Laplacian of the total electron density derived from the experiment (multipole model) and from the HF and DFT calculations is presented in Figure 6 for the Ni complex. The charge concentration (CC) on C−C and C−O bonds and near the oxygen atom toward the nickel ion as well as the lone pair regions of carbonyl oxygen are clearly shown both in experiment and in theory. The local density concentration and depletion around the Ni atom is also clearly shown in Figure 7. The agreement between experiment and theory is adequate; however, the separation between local charge concentration and depletion is much clearer in the experimental ones than that in the theoretical ones. To compare the region near the metal center of all these complexes, the Laplacian of three unique planes around each metal ion is displayed in Figure 8. It is worth noticing that in these figures, the charge concentrations (CCs)

TABLE 5: Properties Associated with Bond Critical Points of $M(C_4O_4)(H_2O)_4$

bond	BL (Å)	metal center	d_1[a] (Å)	$\rho(r_c)$ (e Å^{-3})	$\nabla^2\rho(r_c)$[b] (e Å^{-5})	ϵ[c]	λ_1[d] (e Å^{-5})	λ_2[d] (e Å^{-5})	λ_3[d] (e Å^{-5})
M−O1	2.1076(4)	Fe	1.05	0.40	7.09	0.15			
	2.0767(4)	Co	1.03	0.46	7.36	0.01			
	2.0381(7)	Ni	1.02	0.47	8.07	0.31	−2.32	−1.77	12.16
		Ni[e]	0.97	0.35	10.15	0.06	−1.28	−1.21	12.64
		Ni[f]	0.98	0.38	8.94	0.05	−1.59	−1.52	12.06
	2.0714(6)	Zn	1.03	0.49	7.25	0.05			
M−O3	2.1394(5)	Fe	1.05	0.39	6.84	0.15			
	2.1173(5)	Co	1.06	0.41	6.42	0.10			
	2.0739(7)	Ni	1.03	0.44	7.16	0.18	−2.18	−1.84	11.18
		Ni[e]	0.98	0.32	9.14	0.06	−1.18	−1.11	11.43
		Ni[f]	0.99	0.35	8.15	0.05	−1.39	−1.32	10.86
	2.1202(6)	Zn	1.05	0.44	6.67	0.02			
O1−C1	1.2546(6)	Fe	0.75	2.93	−33.38	0.01			
	1.2538(6)	Co	0.77	2.42	−18.75	0.35			
	1.2532(8)	Ni	0.78	2.52	−21.42	0.20	−25.24	−20.97	24.79
		Ni[e]	0.85	2.23	0.39	0.04	−24.20	−23.18	47.77
		Ni[f]	0.84	2.19	1.54	0.02	−21.14	−20.76	43.44
	1.2546(8)	Zn	0.77	2.82	−29.05	0.16			
C1−C2	1.4627(7)	Fe	0.71	1.89	−13.93	0.12			
	1.4645(6)	Co	0.75	1.80	−12.57	0.25			
	1.4636(9)	Ni	0.75	1.84	−13.88	0.23	−14.13	−11.47	11.72
		Ni[e]	0.75	1.82	−22.53	0.14	−16.25	−14.23	7.96
		Ni[f]	0.75	1.72	−17.96	0.15	−14.56	−12.61	9.21
	1.4628(9)	Zn	0.72	1.84	−11.82	0.20			

[a] d_1 is the distance between BCP to the first atom in the bond. [b] $\nabla^2\rho(r_c) = \lambda_1 + \lambda_2 + \lambda_3$, Laplacian value at CP. [c] $\epsilon = |\lambda_1/\lambda_2| - 1$. [d] λ_1, λ_2, and λ_3 are the Hessian eigenvalues at BCP. λ_3 is along the bond path, and λ_1 and λ_2 are along the direction perpendicular to the bond path. [e] From HF result. [f] From DFT result.

for the metal atom occur in its third quantum shell, and thus are identified with the density of the 3d-orbitals. The pattern of CCs found in the VSCC of the metal atom is a reflection of the uneven populations among five d-orbitals. There are eight lobes of such CCs in the VSCC, located toward the eight triangular faces of the octahedron around the metal center. This geometry can be realized by the linear combination of three t_{2g}-orbitals. Such a feature will give a cubelike domain[59] for the metal (see below in atom domain section).

Bond critical points and the associated properties are given in Table 5. According to these properties, the M−O bond is best described as a closed shell interaction, with $|\lambda_1|/\lambda_3$ much less than 1.0, with $\rho(r_c)$ less than 1.0, and with a positive $\nabla^2\rho(r_c)$ at the BCP, though it was emphasized[60] that this may not be true when the charge distribution is diffused. In this case, we believe that there is some covalent character in the M−O bond, it will be discussed further in the Fermi hole section. On the other hand, for the C_4O_4 ligand, all C−C and C−O bonds are definitely shared interactions, i.e., covalent in character. A large negative $\nabla^2\rho(r_c)$ value and a much greater than 1.0 of $\rho(r_c)$ occur at the BCP. The positive $\nabla^2\rho(r_c)$ of the C−O bond in the MO calculation is rationalized by the electron polarization of such an extremely short bond.[45] The bond ellipticity, ϵ, is a good index for the π-bond character; it is clear that ϵ values of C−C bonds are 0.12−0.25 in experiment, but 0.15 in theory, which is in good agreement with the ϵ value of C−C in benzene (0.23).[45] However, the ϵ values of the C−O bond exhibit a discrepancy between experiment and theory; this is due to the fact that BCP is too close to the C nucleus in theory.[45] The $\rho(r_c)$ value normally correlates well with the bond order; they are 1.8 and 2.6 e Å^{-3}, respectively, for C−C and C−O bonds of squarate, indicating a partial double bond character.

Fermi Hole Function. Bond delocalization is best recognized by the Fermi hole function.[61−63] It was demonstrated[64] that all physical measures of the electron localization or delocalization[65] can be determined by the corresponding localization or delocalization of the Fermi hole density. The Fermi hole density is displayed in Figure 9a−d with the reference electron located

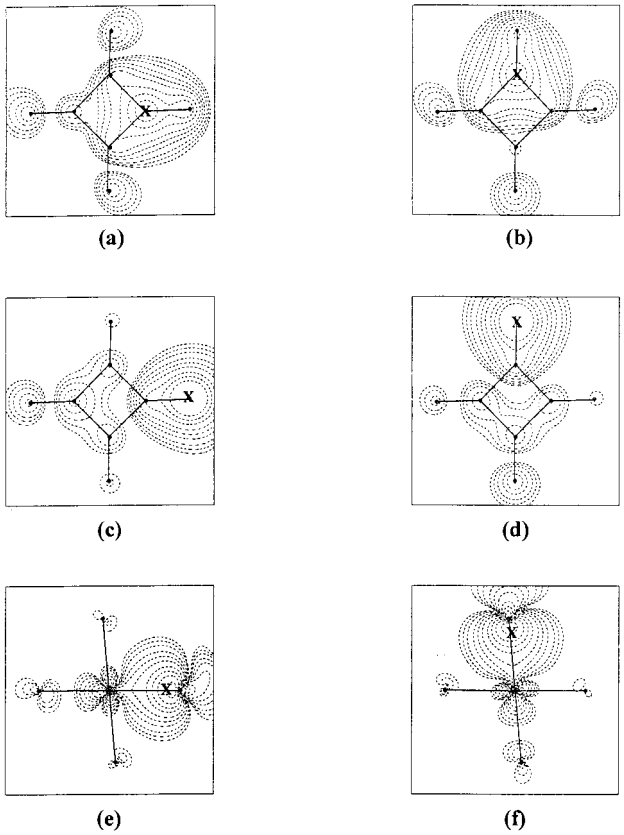

Figure 9. Fermi hole functions from DFT: (a)−(d) at the plane of 0.35 Å above the molecular plane with the reference electron (**x**) placed on this plane at (a) C1, (b) C2, (c) O1, (d) O2; (e), (f) Fermi hole functions at the molecular plane with reference electron situated at (e) O1 in the O1−Ni−O4 plane and (f) O4 in the O1−Ni−O4 plane.

0.35 Å above the squarate plane at various atomic sites. The density indicates the existence of π delocalization of the squarate ligand; however, the density spread in space is covered over the whole ligand when the reference electron is placed on the

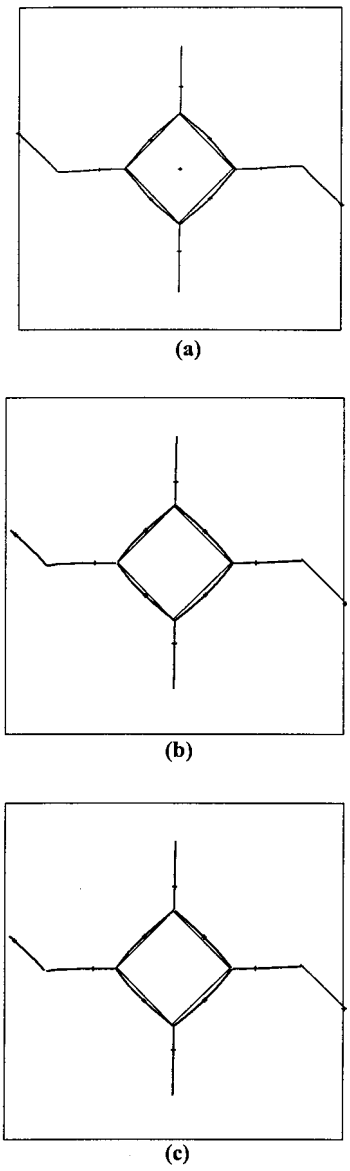

Figure 10. Bond path (with BCP) and interatomic axes of the C_4O_4 plane of the Ni complex from (a) experiment, (b) HF, and (c) DFT.

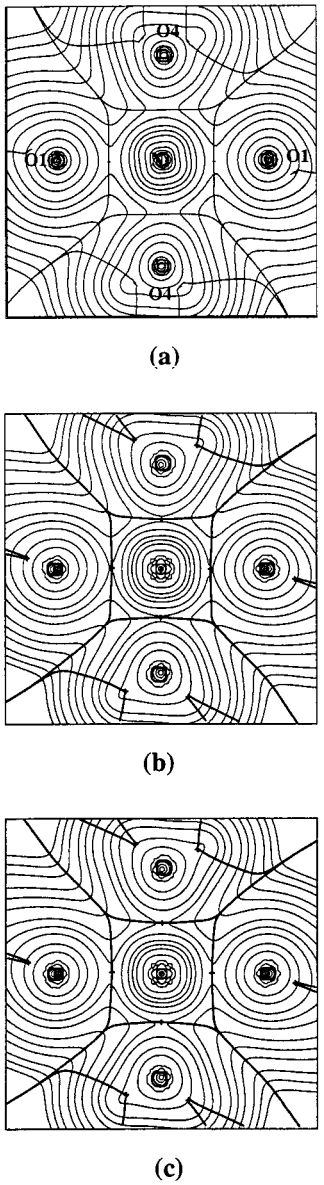

Figure 11. Atom domain and total electron density for the Ni center at the projection of the O1−Ni−O4 plane: (a) experiment; (b) HF; (c) DFT. Contours of electron density are in steps of 2^m10^n e Å^{-3} (m = 1−3; n = −3 to +3).

C atom, while the density spread is only at the C atom and the trans oxygen atom when the reference electron is placed at the oxygen atom. Therefore the delocalization of the p_π-orbital on the ring carbon atoms is more evenly distributed among the C−C bond than that of the C−O bond. These π characters are also consistent with the experimental ϵ values in Table 5.

To probe the M−O σ bond character, a Fermi hole density distribution is plotted in Figure 9e−f with the reference electron located at the lone pair position of oxygen (aq and sq) in the direction of the O−M bond. The distribution clearly indicates the existence of shared character in the $M-O_{sq}$ or $M-O_{aq}$ bond. A similar finding is realized on other transition metal complexes.[46]

Bond Path and Atom Domain. Although the Laplacian of the C_4O_4 plane (Figure 6d−f) does not give so clear an indication of the bent bond as that of deformation density (Figure 5d−f), the C−C bond path does show that the bond path is bent. Figure 10 depicts the bond path together with the interatomic axis (molecular frame) of the C_4O_4 plane from both experiment and theory; the bent feature on the bond path is clearly presented. The atom domain is the partition of molecular electron density into the sum of individual atoms. The atom domain of the metal center in an O_h environment is roughly a cube; one projection is shown in Figure 11 for the Ni complex both from experiment and from theory. The volume of this cube based on the BCP of experiment is 9.3, 9.1, 8.4, and 8.9 Å^3 for Fe, Co, Ni, and Zn, respectively. The smallest one is for Ni, as predicted from ligand field theory.

TABLE 6: d-Orbital Populations of $M(C_4O_4)(H_2O)_4$ (M = Fe, Co, Ni, and Zn)

	Fe	Co	Ni	Ni[a]	Ni[b]	Zn
d_{z^2}	1.09(3)	0.98(4)	0.95(7)	1.09	1.22	1.36(7)
$d_{x^2-y^2}$	1.20(4)	1.11(5)	1.33(8)	1.06	1.15	1.64(8)
d_{xz}	1.43(5)	2.06(6)	2.02(9)	2.01	2.01	1.78(9)
d_{yz}	1.23(4)	1.22(6)	1.71(9)	1.98	2.02	1.55(9)
d_{xy}	1.10(4)	1.51(5)	1.84(8)	2.00	2.01	2.07(8)
total	6.05	6.88	7.89	8.14	8.41	8.40

[a,b] The same as in Table 5.

d-Orbital Populations and Net Atomic Charges. The asphericity in the density distribution around the metal ion can

TABLE 7: Net Atomic Charge of $M(C_4O_4)(H_2O)_4$ (M = Fe, Co, Ni, and Zn)

	Fe	Co	Ni	Ni[a]	Ni[b]	Zn
M	0.28(2)	0.49(5)	0.47(5)	1.66	1.23	1.97(5)
O1	−0.45(2)	−0.39(2)	−0.39(2)	−0.82	−0.60	−0.48(2)
O2	−0.34(2)	−0.30(2)	−0.37(3)	−0.67	−0.51	−0.45(2)
O1′				−0.63	−0.47	
O2′				−0.75	−0.57	
O3	−0.61(2)	−0.53(2)	−0.52(3)	−0.79	−0.67	−0.64(3)
O4	−0.59(2)	−0.55(2)	−0.53(3)	−0.77	−0.66	−0.51(3)
C1	0.10(3)	0.05(3)	0.05(4)	0.44	0.29	−0.13(4)
C2	0.00(3)	−0.09(3)	0.03(4)	0.43	0.27	−0.10(4)
C1′				0.33	0.24	
C2′				0.41	0.26	
H1	0.39(1)	0.37(2)	0.36(2)	0.43	0.36	0.35(2)
H2	0.49(1)	0.40(2)	0.37(2)	0.37	0.34	0.30(2)
H3	0.41(1)	0.38(2)	0.38(2)	0.40	0.37	0.43(2)
H4	0.46(1)	0.41(2)	0.39(2)	0.40	0.37	0.25(2)
H5				0.42	0.37	
C_4O_4	−1.38	−1.45	−1.37	−0.86[c]	−0.72[c]	−2.33
H_2O	0.27, 0.28	0.24, 0.24	0.21, 0.24	0.01, 0.03	0.03, 0.08	0.01, 0.17
$M(H_2O)_4$	1.38	1.45	1.37	1.74	1.46	2.33

[a,b] The same as in Table 5. [c] The charge of the HC_4O_4 unit.

also be illustrated with the d-orbital populations, which can be derived directly from the multipole coefficients,[66] P_{lmp}. They are listed in Table 6. The populations of d-electrons are 6.05, 6.88, 7.89, and 8.40 for Fe(d^6), Co(d^7), Ni(d^8), and Zn(d^{10}), respectively. In the cases of Fe and Co complexes, they are obviously a high-spin configuration, which are in accord with the magnetic measurement.[67] In all four metal complexes, the populations on e_g-orbitals are, in general, less than those on t_{2g}-orbitals. According to the d-orbital population, the population at d_{z^2} is less than that at $d_{x^2-y^2}$, which is rationalized with a M−O1 bond (*z*-direction) being 0.04 Å shorter. However, the theoretical calculations in the Ni case give roughly equal population on these two orbitals. Among t_{2g}-orbitals, the population of d_{xz} is significantly higher than the other two for Fe, Co, and Ni complexes; this may well be explained as having some π character in $M-O_{sq}$. A similar statement was mentioned in Tutton salt.[3−5] For the Fe complex, the d-orbital population presented here is in remarkable agreement with those of the Tutton salt both from experiment[5] and from local density approximation (LDA)[9b] calculation. Net atomic charges obtained from the charged spherical model (monopole) of all four complexes are reported in Table 7, together with the ones from MO calculation on the Ni complex. The agreement between experiment and theory on the Ni complex is reasonable. Among the four transition metal ions, Fe, Co, and Ni are nearly neutral and Zn is positive [+(1.97(5)]. The charges of the squarate dianion in Fe, Co, and Ni complexes are roughly "−1"; but in the Zn complex, it is "−2". The difference in the charges of squarate is the reflection of Zn being much more positive than the other metal ions, which has the same trend in the Tutton salt for Cu (+1.8) versus the other metal ions (+0.7 to +1.2).[5] The coordinated H_2O molecule is slightly positive, which is similar to the case of the Tutton salts. Overall, one can probably say that electron transfer is from H_2O to the metal center, and then from the metal ion to the squarate dianion. In the Fe Tutton salt, the charge on OD_2 is slightly positive (0.09), ND_4 is +0.6, and Fe and SO_4 are +0.7 and −2.2, respectively,[5] whereas in the Fe squarate complex, both H_2O and Fe are +0.28 and squarate is −1.38.

Conclusion

Charge density studies on a series of isostructures of 3d-transition metal complexes containing d,[6] d,[7] d,[8] and d^{10} successfully illustrate the consistent deformation density and Laplacian features both on the ligand and at the metal ion. The "bent" bond feature of the four-membered carbon ring is clearly demonstrated both by the deformation density map and by the bond path. The π delocalization on the ligand squarate is demonstrated via the Fermi hole function. The bonding between the metal and oxygen is mainly a σ donor from oxygen lone pairs with covalent character. The total number of d-electrons out of experiment is 6.05, 6.88, 7.89, and 8.40 for Fe, Co, Ni, and Zn, respectively. The asphericity in density near the metal ion is apparent. The agreement between the experiment and theory on the Ni complex is reasonable. The atom domain of the metal ion is 9.3, 9.1, 8.4, and 8.9 $Å^3$ for Fe, Co, Ni, and Zn, respectively.

Acknowledgment. The authors would like to thank the National Science Council of ROC for financial support and NCHC for making the computers and software avaiable. Thanks are due to Professor Bader and Professor Souhassou for their kindly supplying the necessary softwares.

Supporting Information Available: Multipole coefficients, P_{lmp}, of four compounds (Table IS−IVS) are available free of charge via the Internet at http://pubs.acs.org.

References and Notes

(1) Maslen, E. N.; Ridout, S. C.; Watson, K. J. *Acta Crystallogr.* **1988**, *B44*, 96.

(2) Maslen, E. N.; Watson, K. J.; Moore, F. H. *Acta Crystallogr.* **1988**, *B44*, 102.

(3) Figgis, B. N.; Kucharski, E. S.; Reynolds, P. A. *Acta Crystallogr.* **1990**, *B46*, 577.

(4) (a) Figgis, B. N.; Khor, L.; Kucharski, E. S.; Reynolds, P. A. *Acta Crystallogr.* **1992**, *B48*, 144. (b) Figgis, B. N.; Iversen, B. B.; Larsen, F. K.; Reynolds, P. A. *Acta Crystallogr.* **1993**, *B49*, 794.

(5) Figgis, B. N.; Kepert, C. J.; Kucharski, E. S.; Reynolds, P. A. *Acta Crystallogr.* **1992**, *B48*, 753.

(6) Hester, J. R.; Maslen, E. N.; Glazer, A. M.; Stadnicka, K. *Acta Crystallogr.* **1993**, *B49*, 641.

(7) Kellersohn, T.; Delaplane, R. G.; Olovsson, I.; McIntyre, G. J. *Acta Crystallogr.* **1993**, *B49*, 179.

(8) Ptasiewicz-Bak, H.; Olovsson, I.; McIntyre, G. J. *Acta Crystallogr.* **1993**, *B49*, 192.

(9) (a) Chandler, G. S.; Christos, G. A.; Figgis, B. N.; Gribble, D. P.; Reynolds, P. A. *J. Chem. Soc., Faraday Trans.* **1992**, *88*, 1953. (b) Chandler, G. S.; Christos, G. A.; Figgis, B. N.; Reynolds, P. A. *J. Chem. Soc., Faraday Trans.* **1992**, *88*, 1961.

(10) Akesson, R.; Pettersson, L. G. M.; Sandström, M.; Siegbahn, P. E. M.; Wahlgren, U. *J. Phys. Chem.* **1992**, *96*, 10773.
(11) Fender, B. E. F.; Figgis, B. N.; Forsyth, J. B.; Reynolds, P. A.; Stevens, E. *Proc. R. Soc. London* **1986**, *A404*, 127.
(12) Deeth, R. J.; Figgis, B. N.; Forsyth, J. B.; Kucharski, E. S.; Reynolds, P. A. *Proc. R. Soc. London* **1989**, *A421*, 153.
(13) Figgis, B. N.; Forsyth, J. B.; Kucharski, E. S.; Reynolds, P. A.; Tasset, F. *Proc. R. Soc. London* **1990**, *A428*, 113.
(14) Reynolds, P. A.; Figgis, B. N.; Kucharski, E. S. Mason, S. A. *Acta Crystallogr.* **1991**, *B47*, 899.
(15) Hjorth, M.; Norrestam, R.; Johansen, H. *Acta Crystallogr.* **1990**, *B46*, 1.
(16) Kellersohn, T.; Delaplane, R. G.; Olovsson, I. *Acta Crystallogr.* **1994**, *B50*, 316.
(17) Yeh, S. K.; Wu, S. Y.; Lee, C. S.; Wang, Y. *Acta Crystallogr.* **1993**, *B49*, 806.
(18) Wang, C. C.; Wang, Y.; Chou, L. K.; Che, C. M. *J. Phys. Chem.* **1995**, *99*, 13899.
(19) Lee, C. S.; Hwang, T. S.; Wang, Y.; Peng, S. M.; Hwang, C. S. *J. Phys. Chem.* **1996**, *100*, 2934.
(20) Montgomery, H.; Chastain, R. V.; Natt, J. J., Witkowska, A. M.; Lingafelter, E. *C. Acta Crystallogr.* **1967**, *22*, 775.
(21) Montgomery, H.; Chastain, R. V.; Lingafelter, E. C. *Acta Crystallogr.* **1966**, *20*, 731.
(22) Grimes, N. W.; Kay, H. F.; Webb, M. W. *Acta Crystallogr.* **1963**, *16*, 823.
(23) Webb, M. W.; Kay, H. F.; Grimesn, N. W. *Acta Crystallogr.* **1965**, *18*, 740.
(24) Brown, G. M.; Chidambaram, R. *Acta Crystallogr.* **1969**, *B25*, 676.
(25) Montgomery, H.; Lingafelter, E. C. *Acta Crystallogr.* **1964**, *17*, 1295.
(26) Frankenbach, G. M.; Beno, M. A.; Kini, A. M.; Williams, J. M.; Welp, U.; Thompson, J. E.; Whangbo, M.-H. *Inorg. Chim. Acta* **1992**, *192*, 195.
(27) Weiss, A.; Riegler, E.; Alt, I.; Bohme, H.; Robl. Ch. *Z. Naturforsch.* **1986**, *41B*, 18.
(28) Weiss, A.; Riegler, E.; Robl. Ch. *Z. Naturforsch.* **1986**, *41B*, 1333.
(29) Robl. Ch.; Weiss, A. *Z. Naturforsch.* **1986**, *41B*, 1341.
(30) Gerstein, B. C.; Habenschuss, M. *J. Appl. Phys.* **1972**, *43*, 5155.
(31) Yaghi, O. M.; Li, G.; Groy, T. L. *J. Chem. Soc., Dalton Trans.* **1995**, 727.
(32) Lee, C. R.; Wang. C. C.; Wang, Y. *Acta Crystallogr.* **1996**, B52, 966.
(33) Wang, Y.; Stucky, G. D.; Williams, J. M. *J. Chem. Soc., Perkin Trans. 2* **1974**, 35.
(34) Semmingsen, D.; Hollander, F. J.; Koetzle, T. F. *J. Chem. Phys.* **1977**, *66*, 4405.
(35) Semmingsen, D. *Tetrahedron Lett.* **1973**, 807.
(36) Cohen, S.; Lacher, J. R.; Park, J. D. *J. Am. Chem. Soc.* **1959**, *81*, 3480.
(37) Semmingsen, D. *Acta Chem. Scand.* **1973**, *27*, 3961.
(38) Wang, Y.; Stucky, G. D. *J. Chem. Soc., Perkin Trans. 2* **1974**, 925.
(39) Lin, K. J.; Cheng, M. C.; Wang, Y. *J. Phys. Chem.* **1994**, *98*, 11685.
(40) Gutschke, S. O. H.; Molinier, M.; Powell, A. K.; Wood, P. T. *Angew. Chem., Int. Ed. Engl.* **1997**, *36*, 991.
(41) Lin, K. J.; Lii, K. H. *Angew Chem., Int. Ed. Engl.* **1997**, *36*, 2076.
(42) Gabe, E. J.; Le Page, Y.; Charland, J.-P.; Lee, F. L.; White, P. S. *J. Appl. Cryst.* **1989**, *22*, 384.
(43) Hansen, N. K.; Coppens, P. *Acta Crystallogr.* **1978**, *A34*, 909.
(44) Ebsworth, E. A.; Connor, J. A.; Turner, J. J. *Oxygen fluorides*; In *Comprehensive Inorganic Chemistry*; Bailar, J. C., Emeleus, H. J., Nyholm, R. S., Trotman-Dickenson, A. F., Eds.; Pergamon Press: Oxford, U.K., 1973; Vol. 2, Chapter 22, Section 5, pp 747−771.
(45) Bader, R. F. W. *Atom in Molecule—A Quantum Theory*; Clarendon Press: Oxford, U.K., 1990.
(46) Hwang, T. S.; Wang, Y. *J. Phys. Chem.* **1998**, *A102*, 3726.
(47) Rappe, A. K.; Smedley, T. A.; Goddard, W. A., III. *J. Phys. Chem.* **1981**, *85*, 2607.
(48) Wachters, A. J. H. *J. Chem. Phys.* **1970**, *52*, 1033.
(49) Becke, A. D. *J Chem. Phys.* **1993**, *98*, 5648.
(50) Pople, J. A.; Head-Gordon, M.; Fox, D. J.; Raghavachari, K.; Curtiss, L. A. *J. Chem. Phys.* **1989**, *90*, 5622.
(51) Curtiss, L. A.; Jones, C.; Trucks, G. W.; Raghavachari, K.; Pople, J. A. *J. Chem. Phys.* **1990**, *93*, 2537.
(52) Perdew, J. P.; Wang, Y. *Phys. Rev.* **1992**, *B45*, 3244.
(53) Gaussian94, (Revision A. 1); Frisch, M. J., Trucks, G. W., Schlegel, H. B., Gill, P. M. W., Johnson, B. G., Robb, M. A., Cheeseman, J. R., Keith, T. A., Petersson, G. A., Montgornery, J. A., Raghavachari, K., Al-Laham, M. A., Zakrzewski, V. G., Martin, R. L., Ortiz, J. V., Foresman, J. B., Cioslowski, J., Stefanov, B. B., Nanayakkara, A., Challacombe, M., Gomperts, R., Fox, D. J., Binkley, J. S., Defrees, D. J., Baker, J., Stewart, J. P., Head-gordon, M., Conzalez, C., Pople, J. A. Gaussian Inc.: Pittsburgh, PA, 1995.
(54) PROP program: A program developed by M. Souhassou, N. K. Hansen, E. Stevens, B. Craven, N. Bouhmeida, N. Ghermani, and C. Lecomte.
(55) AIMPAC: a set of programs for the Theory of Atom in Molecules; Bader, B. F. W., and co-workers, Eds.; McMaster University: Hamilton, Ontario, Canada, 1994.
(56) Cotton, F. A.; Daniels, L. M.; Murillo, C. A.; Quesada, J. F. *Inorg. Chem.* **1993**, *32*, 4861.
(57) (a) Dewar, M. S. *J. Am. Chem. Soc.* **1984**, *106*, 669. (b) Cremer, D. *Tetrahedron* **1988**, *44*, 7427.
(58) Iversen, B. B.; Larsen, F. K.; Figgis, B. N.; Reynolds, P. A. *J. Chem. Soc., Dalton Trans.* **1997**, 2227.
(59) MacDougall, P. J.; Hall, M. B. *ACA Trans.* **1990**, *26*, 105.
(60) Smith, G. T.; Mallinson, P. R.; Frampton, C. S.; Farrugia, L. J.; Peacock, R. D.; Howard, J. A. K. *J. Am. Chem. Soc.* **1997**, *119*, 5028.
(61) McWeeny, R. *Rev. Mod. Phys.* **1960**, *32*, 335.
(62) Bader, R. F. W.; Stephens, M. E. *Chem. Phys. Lett.* **1974**, *26*, 445.
(63) Bader, R. F. W.; Stephens, M. E. *J. Am. Chem. Soc.* **1975**, *97*, 7391.
(64) Bader, R. F. W.; Johnson, S.; Tang, T.-H.; Popelier, P. L. A. *J. Phys. Chem.* **1996**, *100*, 15398.
(65) Bader, R. F. W.; Streitwieser, A.; Neuhaus, A.; Laidig, K. E.; Speers, P. *J. Am. Chem. Soc.* **1996**, *118*, 4959.
(66) Coppens, P. *Coord. Chem. Rev.* **1985**, *65*, 285.
(67) West, R.; Niu, H. Y. *J. Am. Chem. Soc.* **1963**, *85*, 2589.
(68) Larson, A. C. *Crystallographic Computing*; Copenhagen: Munkasgaard, 1970; p 293.